Journal of Materials Processing Tech. 299 (2022) 117376

Contents lists available at ScienceDirect

Journal of Materials Processing Tech.

journal homepage: www.elsevier.com/locate/jmatprotec

Investigating flank face friction during precision micro cutting of commercially pure titanium via plunging tests with diamond grooving tools

Yiğit Karpat [a,b,c,*]

[a] Department of Industrial Engineering, Bilkent University, Ankara, Turkey
[b] UNAM – Institute of Materials Science and Nanotechnology, Turkey
[c] Department of Mechanical Engineering, Bilkent University, Ankara, Turkey

ARTICLE INFO

Associate Editor: Erhan Budak

Keywords:
Cutting
Micro machining
Friction
Size effect

ABSTRACT

This study investigates flank face friction while micro machining commercially pure titanium (cp-Ti grade 2) work material considering size effects. It is important to understand friction phenomena at the tool flank and work material surface since they affect the surface integrity of the machined parts. A single crystal diamond grooving tool is used in machining experiments to reduce the influence of cutting edge radius. In addition, plunging type of cutting experiments were performed to investigate the influence of flank face contact on the machined surface. A friction model which is based on work and tool material properties is proposed to model the contribution of adhesion and deformation of the flank face coefficient of friction. The results show that for the cp-Ti and diamond tool pair, adhesion seems to be the dominant model of friction and also contributes to the size effect. The deformation friction becomes more dominant during the chip formation stage. When cutting edge effect is eliminated, the influences of flank and rake face friction on the size effect are shown.

1. Introduction

Precision micro machining is a critical process for creating necessary micro scale features that add value on products used in critical industries. For example, in biomedical applications, commercially pure titanium (cp-Ti grade 2) exhibits good ductility and excellent corrosion resistance, and precision micro machining helps maintain good surface integrity to improve wear resistance. Additional information about this titanium alloy can be found in Lütjering and Williams (2007). Due to its hexagonal close packed (hcp) crystal structure, its machinability is lower compared to face centered cubic (fcc) metals. In the case of precision machining, where the goal is to obtain superior surface finish, it is important to understand friction phenomena at the tool flank and work material surface. This study investigates the flank face friction while micro machining commercially pure titanium (cp-Ti grade 2) work material considering size effects.

In precision micro machining, it has been shown that maintaining a proper uncut chip thickness to edge radius ratio is crucial to obtaining a fine surface finish. At this scale, the uncut chip thickness (h), the grain size of the material, and the edge radius (r_e) of the cutting tool are all in the same order of magnitude. Lucca et al. (1993) showed that when the uncut chip thickness is low compared to edge radius, a significant increase in specific cutting energy occurs. There is a minimum value of uncut chip thickness (h_{min}) below which continuous chip formation ceases, and if machining is conducted under such conditions, the work material is ploughed and then rubbed on the surface. Rahman et al. (2018) considered the ratio of uncut chip thickness to edge radius (h/r_e), called cutting edge effect, together with material properties and identified favorable ratios that yield the best surface roughness values for different materials. Arcona and Dow (1998) showed that even when diamond tools (with very small edge radius) are used, springback of the deformed material influences the precision machining process depending on the stresses, hardness (H), elastic modulus (E) of the work material, and clearance angle of the tool. Ramos et al. (2012) considered built-up edge formation (BUE) which is commonly observed in micro scale machining, concluding that BUE alters contact conditions and thus affects minimum uncut chip thickness. Childs (2010) conducted finite element-based analysis to investigate size effect in machining. He developed linear functions for ploughing forces which are dependent on shear flow stress and the tool's cutting edge radius, which showed a weak dependency of the ratio of uncut chip thickness to cutting edge radius. Liu and Melkote (2007) investigated the relationship between tool edge radius and size effect through strain gradient plasticity model which was integrated into a finite element simulation of machining.

* Corresponding author at: Bilkent University, Department of Industrial Engineering, Turkey.
E-mail address: ykarpat@bilkent.edu.tr.

https://doi.org/10.1016/j.jmatprotec.2021.117376
Received 2 August 2021; Received in revised form 9 September 2021; Accepted 15 September 2021
Available online 20 September 2021
0924-0136/© 2021 Elsevier B.V. All rights reserved.

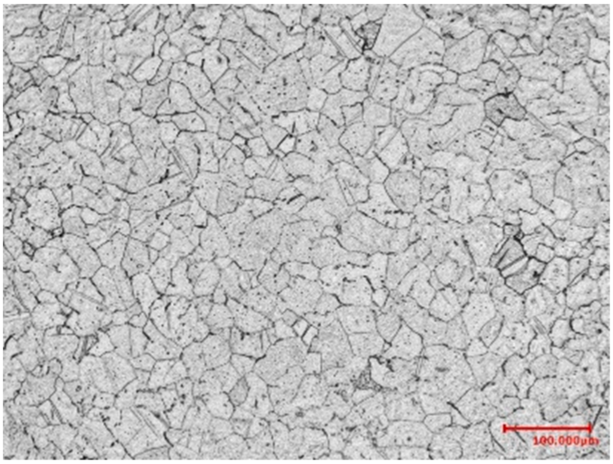

Fig. 1. Equiaxed microstructure of the cp-titanium used in this study.

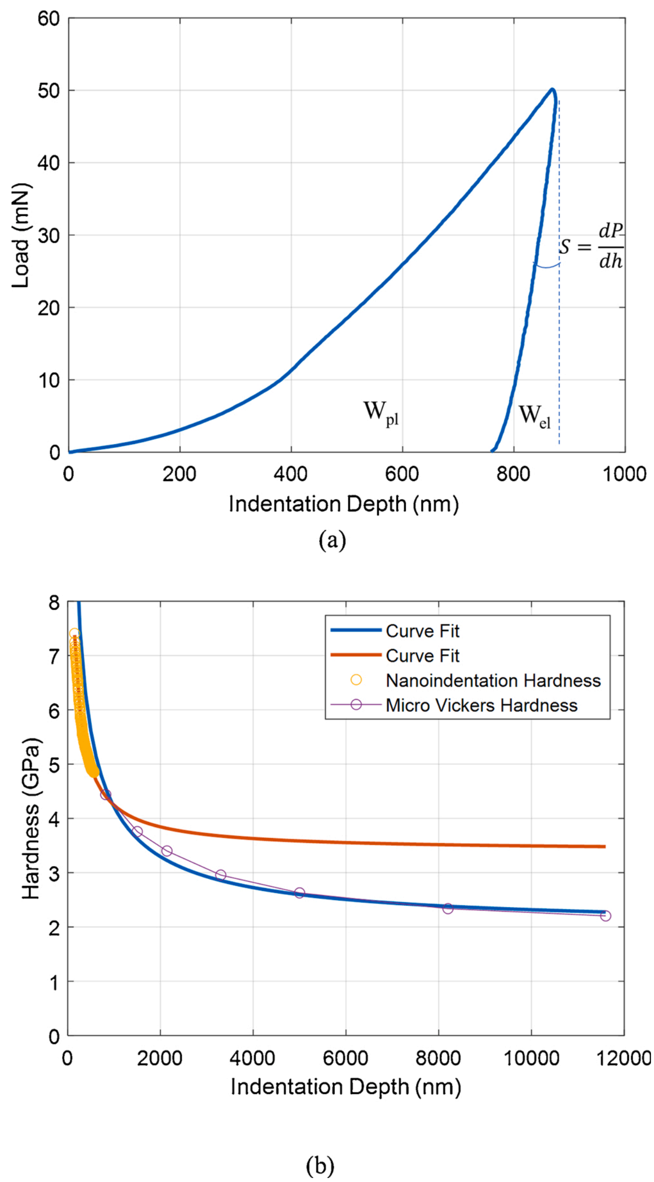

Fig. 2. (a) Nanoindentation test result and (b) hardness measurements as a function of indentation depth.

Their results showed that size effect is due to the intrinsic material dependent length scale and partially on the tool edge radius. The edge radius expands the plastic shear zone and changes the material flow pattern around the tool and hence increases tool-chip contact length. Their results showed a nonlinear increase in specific cutting energy that occurs near the material's length scale. In a recent study, Feng and Sagapuram (2021) investigated the influence of rake face friction on the size effect during machining. In their experiments, they used a glass knife to minimize the edge radius effect. Their result showed a nonlinear increase in specific cutting energy even in the absence of edge radius. They provided a detailed discussion on the size effect in their study.

There is significant amount of contact between the flank face of the tool and the work material during micro scale machining. Friction is considered as the force to shear intermetallic junctions and ploughing of the softer material by the asperities of the harder surface. Friction is known to be system response and it mainly depends on the real area of contact. Greenwood and Williamson (1966) modeled the asperities as spheres having equal radius but exponentially distributed. They assumed that asperities can elastically deform and formulated the real area of contact depending on the load, composite modulus of elasticity (E^*), and texture parameters of the surface. Plastic deformation would begin when the pressure at the asperities is greater than the hardness of the material. They proposed a plasticity index where the material properties (E^*/H) and surface topology parameters are combined to define the elastic and plastic deformation limits where H is the hardness of the surface. However, asperities do not deform independently, and their interactions with each other were not considered in this theory. Persson and Scaraggi (2014) introduced a new contact theory to include interactions of the asperities. He introduced a length scale and used power spectral density information of the surface topology to improve his theory of contact. Suh and Sin (1981) showed that friction force depends on the history of sliding and studied the time-dependent nature of kinetic coefficient of friction. They showed the friction undergoes significant changes during the early stages of contact and considered the influence of loose particles coming off from the surface on the friction. They reported that the coefficient of friction between sliding surfaces is due to the various combined effects of an asperity deformation component, a component from plowing by wear particles and hard surface asperities and a component from adhesion between the flat surfaces. Bhushan and Nosonovsky (2004) considered scale (size) effects in dry friction from macro to nano scale. They considered strain-gradient plasticity, dislocation-assisted sliding, surface roughness, and contamination of the interface by particles as scale effects. Micro hardness and state-of-the-art nanoindentation tests, which is governed by dislocation-based mechanisms under the indenter, can be used to identify material properties. A review of nano indentation size effect in polycrystalline materials can be found in Voyiadjis and Peters (2010). Such tests yield information about the decrease in hardness with increasing indentation depth as function of length scale of the material. This study utilizes micro hardness and nano indentation tests to deduce material properties such as hardness, modulus of elasticity, and the length scale of the material. This information will be used to model adhesion and deformation components of the flank face friction. In a recent study, Melkote et al. (2017) have reviewed the relationship among work material properties and friction modeling and emphasized the importance of developing new experimental methods to investigate friction identification methods.

In this study, the focus is on investigating flank and rake face friction and its relationship with the size effect. A single crystal diamond grooving tool is used in machining experiments to reduce the influence of cutting edge radius on the size effect. In orthogonal machining tests, the cutting tool is continuously fed towards the work material where the same surface is cut over and over in each rotation of the specimen. Therefore, the mechanical properties of the surface layer (dislocation density) may be influential in the next cycle. In order to eliminate that effect, plunging type grooving tests were performed on an ultra-

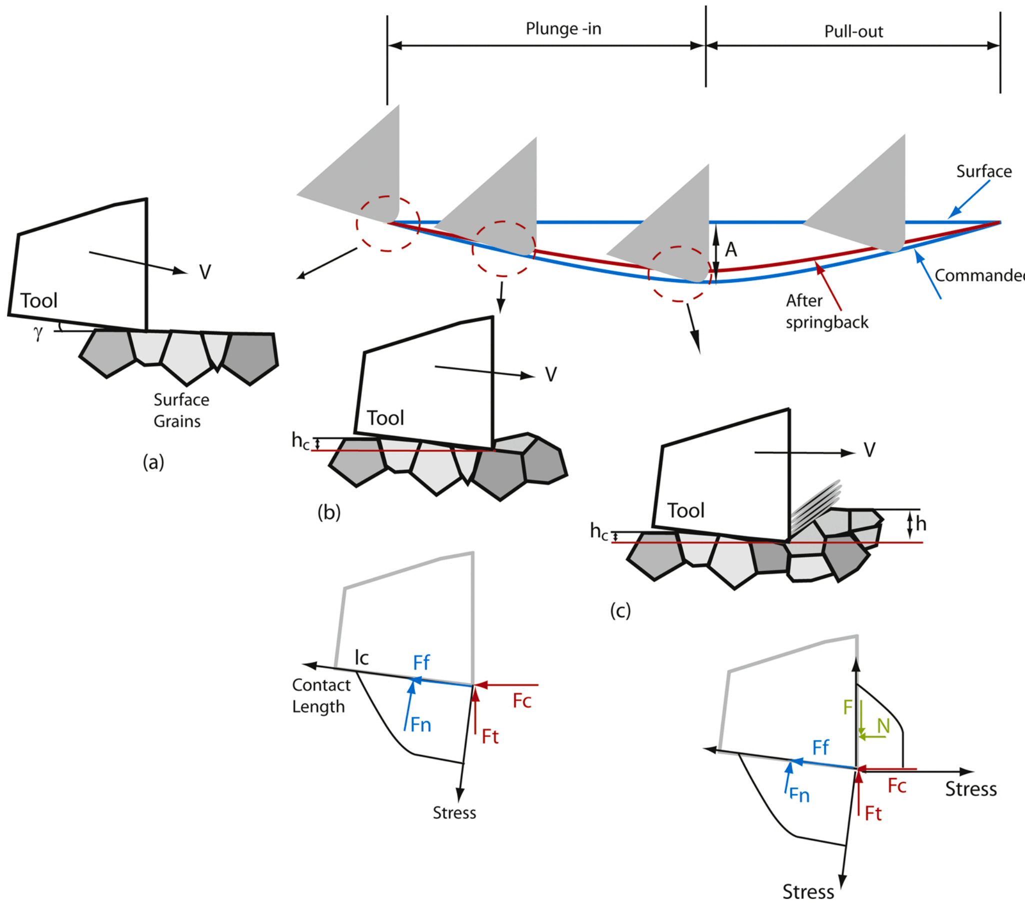

Fig. 3. Experimental method to identify flank and rake face friction. (a) Initial contact of the tool tip, (b) Interaction of the flank face of the tool with the work material and material pile up in front of the tool. Forces acting on the flank face of the tool and corresponding stress distribution, (c) Initiation of the chip formation and stress distributions on the rake and flank faces together with forces.

precision CNC machine such that the work material surface is cut only once during the machining cycle. This approach also limits temperature rise and prevents BUE formation, which simplifies the complex friction identification problem. The analysis includes machining force measurements and a surface topology investigation. Depending on the diameter of the work material, the extended length of cutting allows for investigating the time history of flank and rake face coefficient of friction due to adhesion and ploughing. A model has been developed to analyze the contribution of each to the flank face friction.

2. Work material properties and investigating indentation size effect on cp-Ti

In this study, commercially pure titanium (cp-Ti grade 2) has been considered due to its practical importance, which is an alpha alloy with hexagonal close packed crystal structure. Its low elastic modulus also allows for investigating the flank contact. The chemical composition of the annealed (ASTM B348 B381) cp-Ti having equiaxed microstructure with 25 μm grain size (as shown in Fig. 1) consists of C%0.08, N%0.03, O%0.25, Fe%0.3, H%0.015, according to the material certificate provided by the vendor. It has tensile strength of 604 MPa and yield strength of 453 MPa. The cp-Ti sample used in this study is 50 mm in diameter and its surface was diamond turned on a CNC ultra-precision machine tool where the rotational speed was kept at 400 rpm with 5 mm/min feed rate. A diamond cutting tool with 0 ° rake angle and 0.85 mm nose radius was used in the face turning process. A laser topography microscope (Keyence VKX 100) was used to measure the initial surface topography and the rms areal surface roughness (S_q) was measured as 140 nm.

Nanoindentation tests were performed under different conditions with a Berkovich indenter. The surfaces were electropolished before the nano indentation experiments. A total of 15 tests were performed with loads ranging from 50 mN to 200 mN with 100 mN/min loading/unloading rate including a 5 s pause at the peak load (CSM NHT2 Nanoindenter). Fig. 2(a) shows the load vs displacement graph obtained from the test. The area under the curve can be used to identify the plastic and elastic work during indentation test and a ratio of elastic work to total work (W_e/W_t) was measured between 0.1−0.2 through the tests. The average modulus of elasticity of the material was measured as E = 115 GPa from the unloading curve. Novikov et al. (1996) showed that loading curve of the nano-indentation test can be used to calculate the average contact pressure by Eqs. (1) and (2) where P_i is the instantaneous load, h_i is the instantaneous displacement, and the term S represents the unloading stiffness. Considering the definition of hardness as load divided by indentation area, the average contact pressure can be calculated and the hardness values obtained from nanoindentaton tests as shown in Fig. 2(b).

$$h_{c_i} = h_i - 0.75\frac{P_{max}}{S}\sqrt{\frac{P_i}{P_{max}}} \tag{1}$$

$$P_{ave,i} = \frac{P_i}{24.5h_{ci}^2} \tag{2}$$

The results clearly show that with decreasing indentation depth, the hardness of the material increases, and this is known as the indentation size effect (ISE). The movements of geometrically necessary dislocations (GND) are blocked by grain boundaries in polycrystalline materials. At grain boundaries dislocations, pile-up, and local hardening is observed

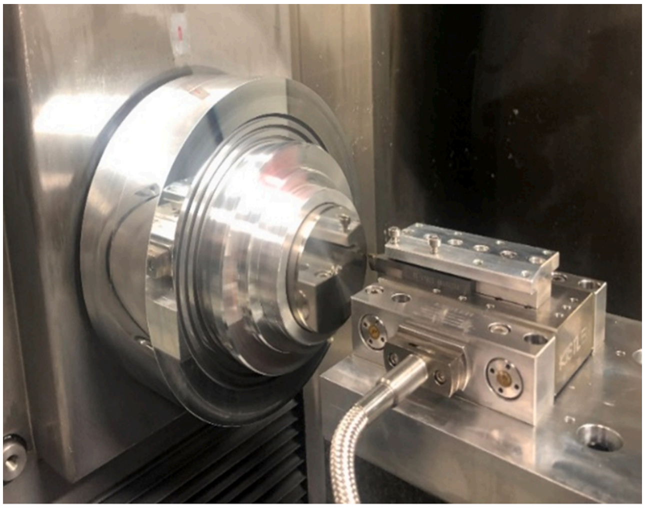

(a)

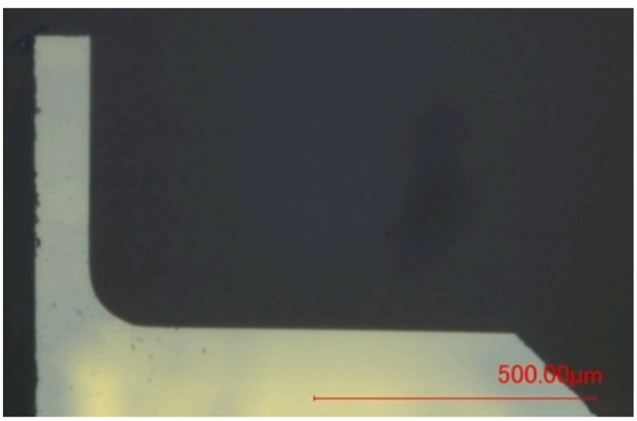

(b)

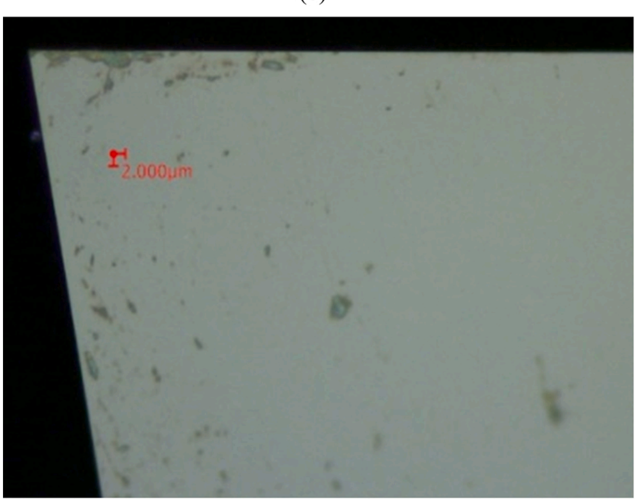

(c)

Fig. 4. (a) CNC ultra-precision machine tool, (b) Diamond grooving tool micro geometry, (c) Cutting edge of the diamond grooving tool.

Table 1
Planning of Plunge-in/Pull-out tests.

Amplitude (µm)	Radius and Rotational Speed
2	18.4 mm–346 rpm
3	18.26 mm–348 rpm
5	18.12 mm–351 rpm

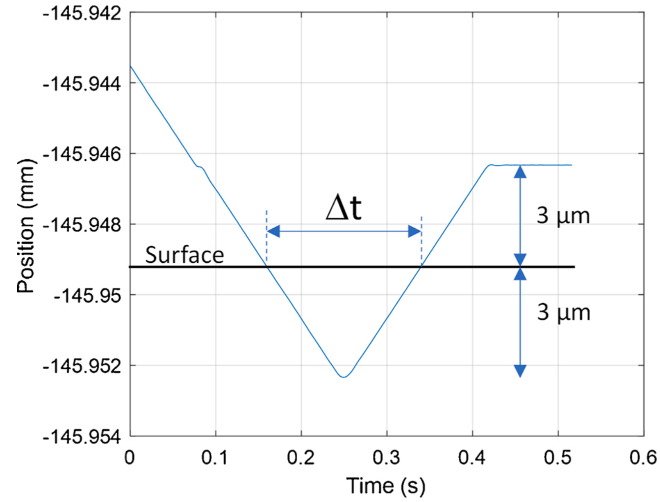

(a)

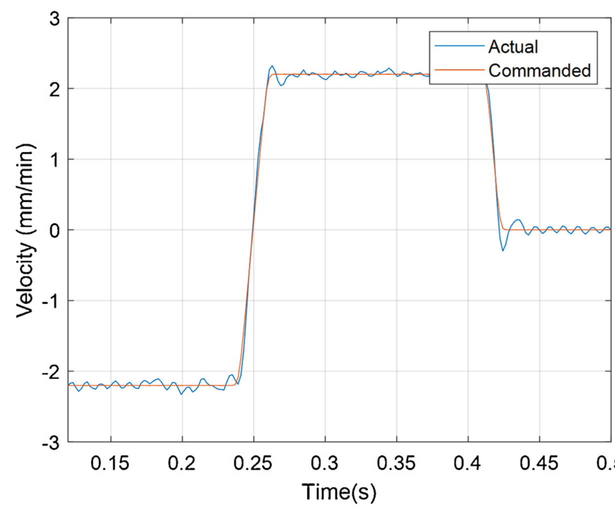

(b)

Fig. 5. (a) Actual position and (b) velocity measurements from the machine.

due to this resistance. When the dislocation density reaches a critical value, dislocations can move on to the next grain, and the size effect curve follows the conventional size effect response. Grain morphology of the material would also affect the process considering the grain orientation and existing dislocations inside the grain. Micro Vickers testing was also used to measure the hardness of the work material under different loadings (0.01, 0.025, 0.05, 0.1, 0.2, 0.5 and 1 kgf). Each test was repeated at three different locations on the diamond machined surface. Indentation depth was measured using laser surface topography microscope. Those measurements are also shown in Fig. 2(b).

The generalized indentation hardness–depth relation established by Huang et al. (2006) is shown in Eq. (3) where H_0 is the macro scale hardness with no size effect and h^* is the length scale of the material where size effect diminishes. Eq. (3) cannot effectively represent both micro hardness and nano indentation tests at the same time due to indenter tip radius effect at low depths. Therefore, two different length scales and macro hardness values can be calculated. Based on micro-Vickers hardness tests, the scale length of the material was identified to be around $h^* = 3.4$ µm, and the macroscale hardness of the material was calculated as $H_0 = 2$ GPa which is around three times the tensile strength of the material. Based on nanoindentation tests, the

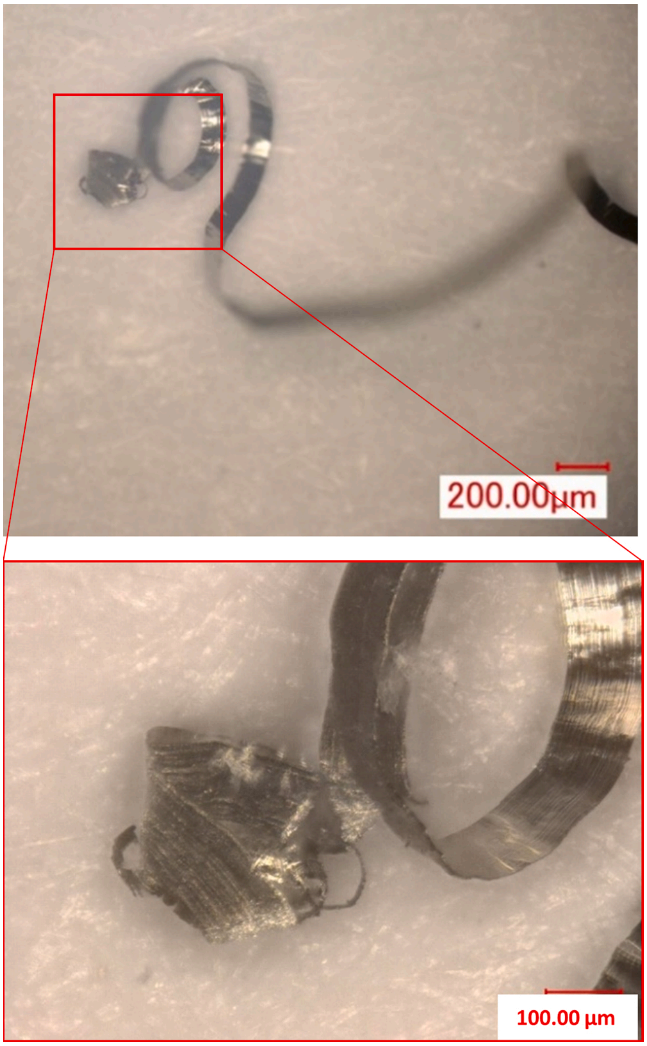

Fig. 6. Diamond tool plunging test chip measurements for 3 µm at different magnifications.

scale length was measured as 550 nm and the macro scale hardness was calculated as 3.4 GPa. Nano indentation and micro scale machining are different processes, yet the initial contact of the flank face of the tool would resemble an indentation process which will be explained in the next section.

$$H = H_0\sqrt{1 + \left(\frac{h^*}{h}\right)} \tag{3}$$

3. Friction modeling in micro scale cutting

This study conducted plunge-in and pull-out type of machining experiments. Fig. 3 shows the stages of the micro machining process where the tip of the tool approaches the work material, plunge-in and performs machining, after reaching the maximum depth, it pulls-out and finally departs from the surface. Fig. 3(a) shows the tip of the tool which interacts with the surface grains of the material. At this point, there is no contact between the tool flank and the work material. In Fig. 3(b), the tip of the tool and the flank face of the tool contacts the material. The interaction will be among the flank face of the tool and the asperities on the surface. The initial surface topology of the work material would determine the initial contact conditions until the flank face fully plunges into the work material. As the tool continues to plunge in, the real contact area on the flank face will increase and the deformations of the asperities will move from elastic to elastic-plastic. At this phase, the elastic modulus and mechanical properties of the work material (E/H ratio) determine the contact conditions as suggested in Arcona and Dow (1998). As the tool moves from one grain to another, dislocation mechanisms as a function of crystal orientation of the grains will also be effective on the contact conditions. In addition, a small amount of material will start accumulating in front of the tool with no complete chip formation. The forces acting on the flank face are shown as friction force (F_f) and the normal force (F_n). Cutting (F_c) and thrust (F_t) forces (measured by a dynamometer) can be transformed into flank face friction force (F_f) and normal force (F_n) as a function of clearance angle (γ) using Eq. (4). Flank face coefficient of friction (μ_f) can be written as in Eq. (5). Friction force on the flank face (μ_f) can considered due to adhesion (μ_a) and ploughing (μ_p) as Eq. (5). The forces and the stress distributions on the flank face are also shown Fig. 3(b).

$$\begin{bmatrix} F_f \\ F_n \end{bmatrix} = \begin{bmatrix} \cos\gamma & -\sin\gamma \\ \sin\gamma & \cos\gamma \end{bmatrix}^{-1} \begin{bmatrix} F_c \\ F_t \end{bmatrix} \tag{4}$$

$$\mu_f = \frac{F_f}{F_n} = \mu_a + \mu_p \tag{5}$$

The relationship between total contact length (l_c) and the contact height (h_c) on the flank face can be written as a function of clearance angle as in Eq. (6). The total height can be represented as contributions of plastic (h_p) and elastic (h_{el}) deformations. Once the tool is removed, the plastic deformation will remain on the surface and the material will relax with the amount of elastic deformation. The contact length can be estimated based on the clearance angle (γ) using Eq. (7).

$$h_c = h_p + h_{el} \tag{6}$$

$$l_c = h_c/\sin\gamma \tag{7}$$

At one point, a critical amount of material will accumulate in front of the tool and micro chip formation will start as shown in Fig. 3(c). A certain uncut chip thickness must be achieved to obtain complete chip formation. In some cases, incomplete micro scale chips may be formed which are difficult to observe during tests. In addition to forces on the flank face, normal (*N*) and friction (*F*) forces will be acting on the rake face as well.

Eq. (8) shows the components of flank face friction force where the first term defines adhesion component with A_r is the real area of contact and τ_s is the adhesion shear strength of the material. The second term is due to deformation which is based on ploughing coefficient of friction and the normal force acting on the surface. If both sides of the Eq. (8) is divided by normal force, flank face coefficient of friction can be rewritten as Eq. (9) as in Bhushan and Nosonovsky (2004). Normal force can be related to hardness of the material together with area of contact. Therefore, the size effect can be included in Eq. (10). The term (H_0/E^*) represent the influence of different work-tool material pairs (Shugurov et al. (2018)). The coefficients C_a and C_p are required to include the surface topology effect on the friction coefficient (Bhushan and Nosonovsky (2004)). The parameters l_s, h_s, h_w, and *m* are material dependent coefficients. When the flank face of the tool comes into contact with the work material surface (Fig. 3(b)), the adhesion component would be high due to size effect. As the tool plunges in further, the amount of deformation would increase. In the next section, the flank face friction including size effect will be investigated through an experimental method.

$$F_f = A_r\tau_s + \mu_p F_n \tag{8}$$

$$\frac{F_f}{F_n} = \frac{A_r\tau_s}{A_r H} + \mu_p \tag{9}$$

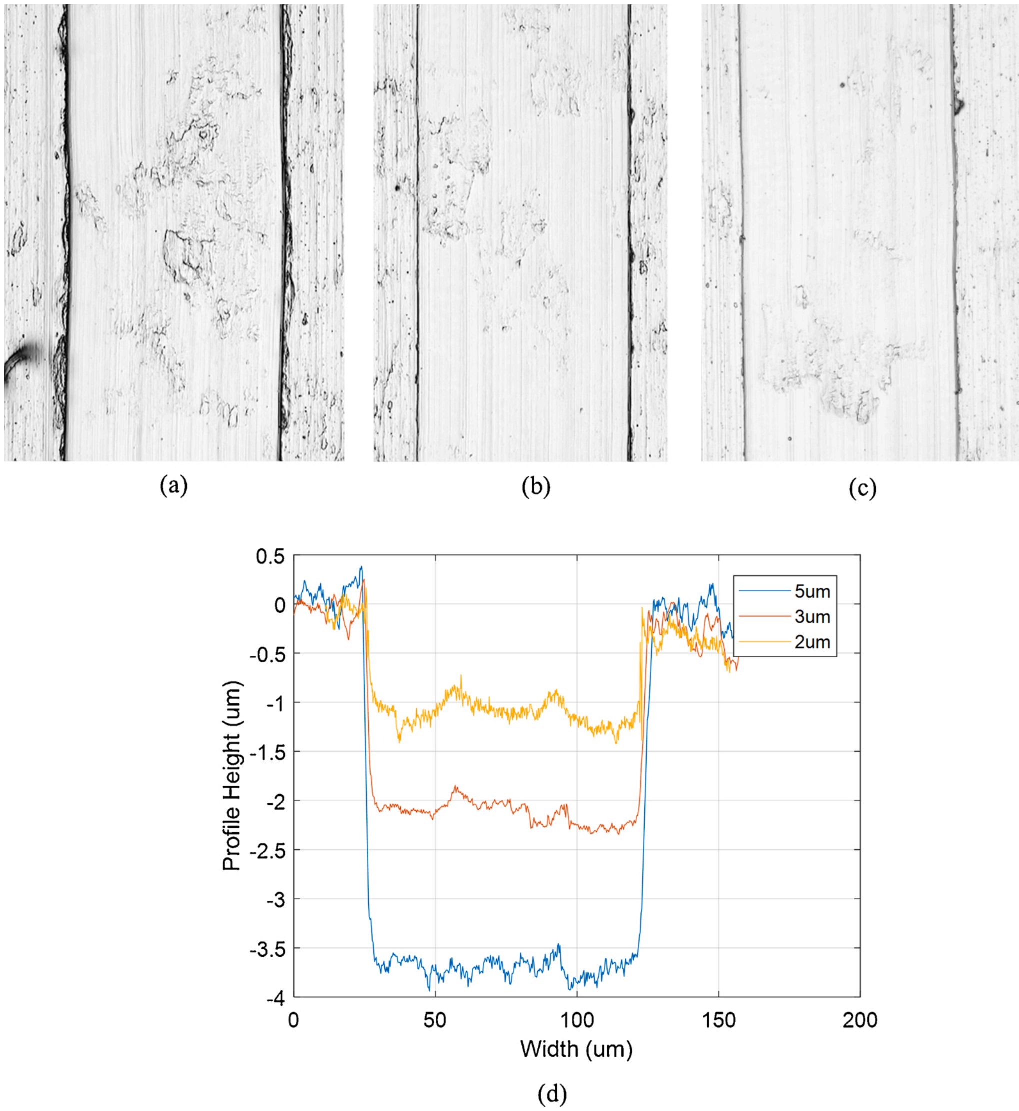

Fig. 7. Profiles of the grooves corresponding to different amplitudes (a) 5 μm, (b) 3 μm, (c)2 μm, (d) Groove profiles corresponding to the deepest section of the channel.

$$\mu_f = C_a \frac{\tau_0 \sqrt{1 + \left(\frac{l_s}{l_c}\right)}}{H_0 \sqrt{1 + \left(\frac{h_s}{h_c}\right)}} + C_p \left(\frac{H_0}{E*}\right) \left(\frac{h_c}{h_w}\right)^m \tag{10}$$

For the last phase of the process as shown in Fig. 3(c), effective coefficient of friction on the rake face can be calculated by subtracting ploughing forces from measured cutting and thrust forces considering the rake angle of the tool (α) as reported in Albrecht (1960). This calculation assumes that the ploughing forces and rake face forces are decoupled.

$$\mu_{rake} = \frac{(F_t - F_{t_p}) + (F_c - F_{c_p})\tan\alpha}{(F_c - F_{c_p}) - (F_t - F_{t_p})\tan\alpha} \tag{11}$$

4. Experimental

Machining tests were conducted on the cp-Ti sample using an ultra-precision turning machine (Moore Nanotech FG350). Fig. 4(a) shows the experimental setup and Fig. 4(b) and (c) show the micro geometry of the diamond grooving tool as measured by laser topography microscope (Keyence VKX 100).

Cutting and thrust forces were recorded by a dynamometer (Kistler 9256C1) with a sampling rate of 333 kHz (NI 7854R A/D converter). Cutting speed was kept constant at 40 m/min in all the experiments. The diamond tool has a width of 100 μm with 10 ° clearance angle and the edge radius is around 50−60 nm as specified by the tool manufacturer (UPC Nano-ALMT tools). The single crystal diamond cutting tool has a rms areal surface roughness (Sq) measurement of 15 nm on the flank face.

In this study, cutting tool is given a sinusoidal trajectory (z=*A*.sin (ωt+π/2)) with an appropriate feed rate so that it plunges-in and pulls-out of the workpiece within one full rotation. Similar experiments were conducted in the literature (Ramos et al. (2012); Zhao et al. (2020)). To define the trajectory of the tool, the amplitude (*A*), and the rotational speed of the workpiece (ω) are required. The rotational speed and feed must be selected in accordance with the radius where a micro-groove will be created. Table 1 shows the experimental conditions used in this study. It is crucial to make sure that the cutting edge of the grooving tool is placed parallel to the work material surface to maintain plunging of the whole width of the tool all at once. Three different amplitudes were selected as 2, 3, and 5 μm. The feed rate was set as 2.2 mm/min such that at 2 and 3 μm amplitudes, the machining was planned to be completed within a single rotation of the work material. Experiments

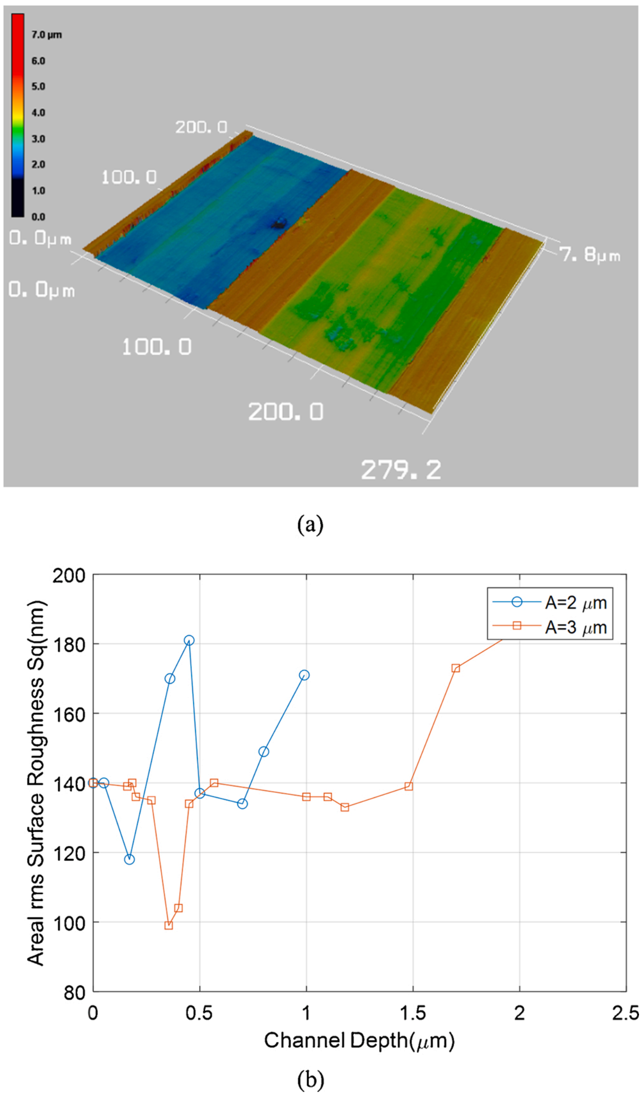

Fig. 8. (a) Surface topology of the machined surface, (b) Areal surface roughness measurements for 2 and 3 μm amplitude and 2.2 mm/min feed rate as function of groove depth.

were repeated three times.

To check whether CNC machine tool can follow the commanded motion, the difference between commanded and actual position (following error) was measured during actual machining tests by accessing to the controller (Delta-Tau PMAC) of the CNC machine. Measurements with sampling rate of 1 ms was used. Fig. 5(a) shows the position and Fig. 5(b) shows the velocity measurements of the z-axis for 3 μm amplitude case. The location of the surface is shown in Fig. 5(a) and Δt shows the time interval, where the plunge-in and pull-out phases must be completed before the work material makes one full rotation.

5. Experimental investigation of process outputs

5.1. Investigating surface integrity

Fig. 6 shows the continuous chip formed during 3 μm amplitude test. The chip is significantly curled at the beginning indicating tangling of the chip before the cutting edge at an earlier phase of the cut as indicated in Fig. 3(b–c). With increasing uncut chip thickness as the tool plunges in, the chip curl radius increases, and similarly the chip curl radius decreases during pull-out. No complete chip formation was observed during 2 μm amplitude machining tests, which indicates that flank face contact was dominant in this condition. No BUE was observed on the tool after the cutting tests.

Fig. 7 shows the grooves machined on the work material at their deepest heights for all cases. The machined surfaces were investigated with a laser topography microscope at various locations and the surface roughness was measured. Maximum values of the measured depths for 2 μm amplitude was around 1.2 μm (ratio of 0.6); for 3 μm amplitude, it was around 2.2 μm (ratio of 0.73), and for 5 μm amplitude, it was measured around 3.7 μm (ratio of 0.74). According to the nanoindentation test results, reported in Section 3, the ratio of plastic work to total work was measured to be around 80 %. At larger amplitudes, the values seem to be in accordance with nanoindentation test results. In α-titanium, deformation modes are governed by the activation of complex slip and twinning modes based on the microstructure. The influence of grain structure of the material can also be observed on the surfaces of the machined grooves considering hcp structure of the cp-Ti material. Deep grain pull-outs were observed on the surface, which possibly occur due to combined effect of unfavorable orientation of the grains with respect to cutting direction together with loading at that region grooves for 2 and 3 μm amplitudes. Similar observations were reported in Kieren-Ehses et al. (2021). It seems to be a dominant factor at 5 μm amplitude machining case as in Fig. 7(a).

Fig. 8(a) shows the topology of the grooves for 2 and 3 μm amplitudes. Fig. 8(b) shows rms areal surface roughness (S_q) parameter measured at different locations along the channels.

The profiles of the machined grooves show peaks and valleys which is a combined result of tool edge profile, plastic deformations, ploughing of loose asperities, material smearing, material swelling, and process dynamics. The initial areal surface roughness is 140 nm. The best surface roughness was obtained around 0.2 μm depth for 2 μm amplitude where the surface finish was improved from initial 140 nm down to 118 nm. For 3 μm amplitude, the best surface finish was obtained around 0.4 μm depth where the rms surface roughness was 100 nm. For the 2 μm amplitude test, the surface roughness rapidly deteriorates as the tool plunges in further. While the edge radius of the tool is in the order of nanometers, the interaction of the tool and work material on the flank face seems to affect the surface quality. For 3 μm amplitude, a similar trend was also observed, yet the variation of surface roughness was stable between 0.5–1.5 μm depth. For 5 μm amplitude, the S_q values were larger than 200 nm.

5.2. Investigating cutting and thrust forces

As described in Fig. 3, as the tool plunges-in, the first contact will occur on the flank face of the diamond tool, which has a smoother surface than the work material. With increasing uncut chip thickness, material will accumulate in front of the tool, and chip formation will initiate once a critical depth is reached. Fig. 9 shows the force measurements for all amplitudes after applying a low pass filter of 1000 Hz. As expected, cutting and thrust force measurements increase with increasing uncut chip thickness and their peak values occur at the deepest point on the grooves. Plunge-in and pull-out force measurement trends are observed to be similar but not identical. In Fig. 9(c), at 5 μm amplitude, around 0.225 s re-entry into the cut was observed, which was identified with a significant peak on thrust and cutting forces.

For better comparison of forces recorded during plunge-in period, Fig. 10 shows measured forces for all cases superposed. Cutting forces increase linearly with increasing uncut chip thickness as the rate of increase (slope of the curve) is quite close for each test. It is important to notice that the intercept of the cutting forces is not a positive value.

As for thrust forces, the rate of increase is high at the beginning, indicated in the figure as Region I. This is the region where the flank face of the tool comes in contact with the work material and elastic and plastic deformations take place. The real area of contact will increase, and the material size effect influences the friction conditions. At Region II, thrust forces increase at a slower rate. This is the region where the size

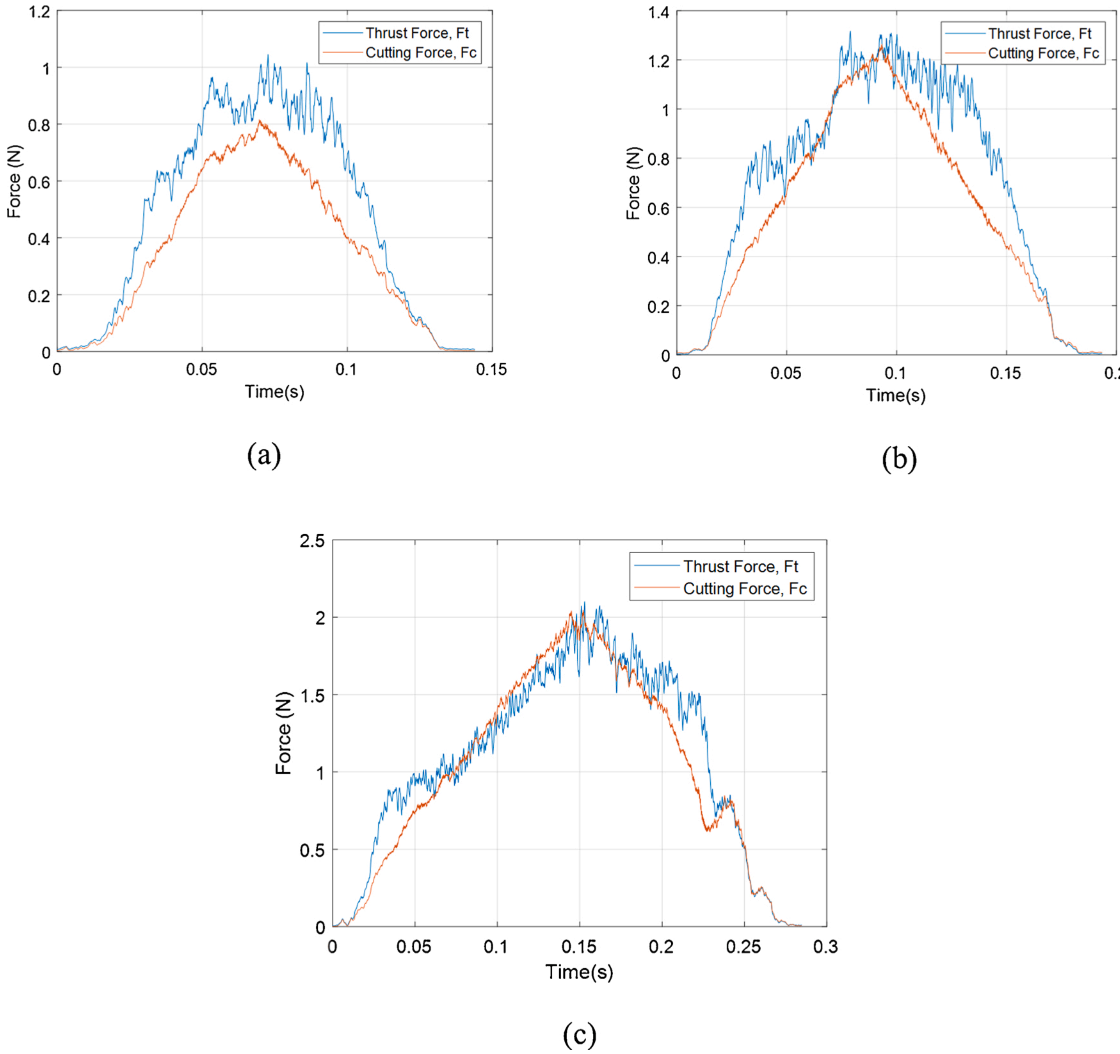

Fig. 9. Force measurements at (a) 2, (b) 3, (c) 5 μm amplitude.

effect diminishes, and some micro-chip formation will initiate in front of the tool with some contact on the rake face, yet it may not be complete chip formation. In Region III, chip formation will occur and thrust force starts to increase due to additional contact on the rake face of the tool. During machining, a significant part of the total energy is converted into heat, some part of the energy is stored inside the material causing changes in the microstructure, and some part of the energy is spent to create a new surface. In a recent study, Zhao et al. (2020) investigated the influence of temperature increase during ultra-precision turning of titanium alloy Ti6Al4V by conducting slow speed servo machining experiments using nose radiused diamond tools. They observed that decreasing elastic modulus of the material with temperature rise during machining creates a larger contact area at the flank face, which is responsible for larger thrust forces. According to data provided in their study, temperature rise must be more than 300 °C which leads to 10 % decrease in modulus of elasticity. In our experiments, we assume that temperature rise would not reach such levels during plunge-in considering the short amount of time and the small width of the diamond grooving tool. Temperature models available in the literature may be integrated into the machining models to study temperature's effect on the frictions.

6. Identifying friction model parameters considering size effect

Forces are shown as a function of tool tip position in Fig. 11. A power equation fit to thrust force was shown for 2 μm amplitude in Region I, where the thrust force curve follows a trend similar to nanoindentation tests indicating an elastic-plastic deformation zone. Around 0.8−1 μm, thrust force measurement departs from the curve fit and switches to a different behavior, indicated as Region II.

For Regions I and II, measured cutting and thrust forces are transformed to friction and normal forces on the flank face of the tool as explained in Eq. (4). It is assumed that all contact occurs at the flank face of the tool. Flank face coefficient of friction can be calculated based on these forces. Fig. 12 shows the variation of flank face coefficient of friction for all cases as a function of tool tip position (h). As the flank face of the tool contacts the work material, adhesion friction is likely to occur. Frictional force increases with increasing area of contact yet the coefficient of friction decreases due to size effect depending on the length scale of the material. For plastic deformation to occur, stress concentration on the surface must be larger than the yield strength of the material considering the scale effects (strain gradient plasticity). As the tool plunges in further, influence of ploughing deformation increases and the trend of coefficient friction changes. Increasing plastic deformation and possible fracturing in the grains would create some loose particles which result in a third body deformation mechanism affecting the machined surface topology, which is observed as scratches (lay) on the surface as shown in Fig. 7 (a, b, c). Increasing surface roughness parameters would also affect the contact conditions on the flank face.

Eq. (10) can be used to represent the data in Fig. 12 and to study the

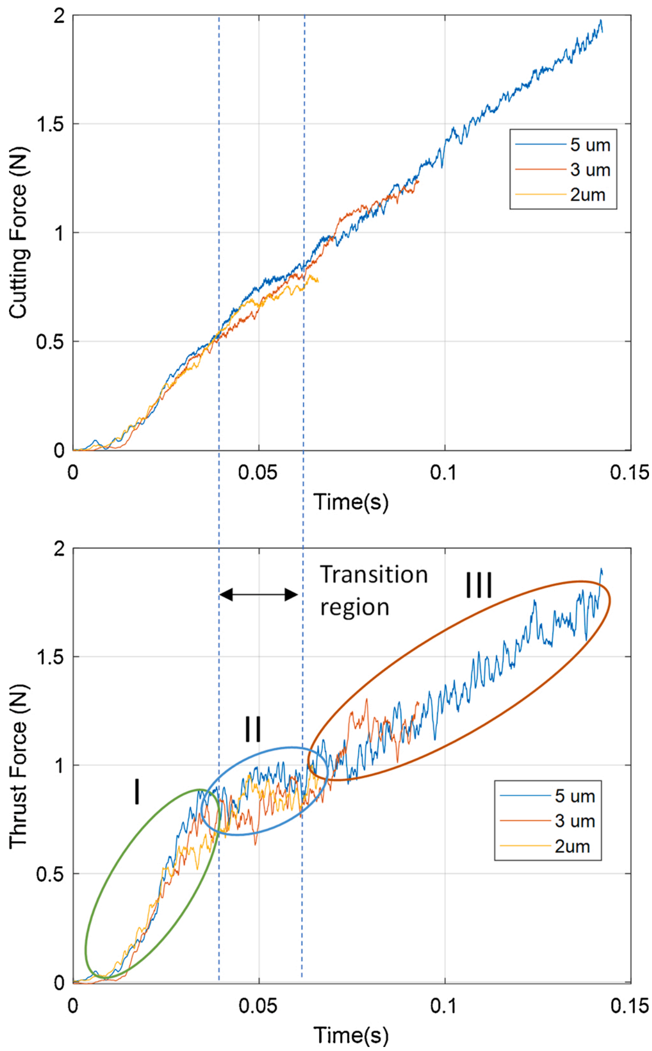

Fig. 10. Comparison of force measurements during plunge-in for 2, 3, 5 μm amplitude.

contribution of adhesion and ploughing friction mechanisms separately. We assume that the macro scale hardness is $H_0 = 2$ GPa as measured in Section 2. It must be noticed that the geometry of the single crystal diamond tool used in machining tests differs from the indenters used in hardness testing. The coefficients m, C_a, and C_p are unknown parameters that are introduced to reflect these differences depending on the length scales. The length scale of hardness size effect is adopted from the nano indentation test results. The length scale for deformation is adapted as 0.8 μm based on the machining test results at the limit of Region I, which is a function of the tool and work material properties. The length scale for shear strength is assumed to depend on the contact length on the flank face of the diamond tool and it is assumed to be 5 μm. An optimization algorithm is used to calculate the unknowns and these are shown in Table 2. It is assumed that the influence of deformation is zero at the beginning of contact. A good fit between the experiment and the model is obtained as shown in Fig. 12, which shows the contribution of adhesion (μa) and deformation (or ploughing) (μp) on the flank face friction.

Based on the results, the contribution of adhesion to the flank face friction seems to be higher than the deformation. The low surface roughness of the diamond tool must influence this result considering the real contact area. The coefficient *m* controls the influence of deformation towards the end of the contact which is calculated to be lower at the low amplitude test case of 2 μm. The C_a and C_p parameters are almost equal

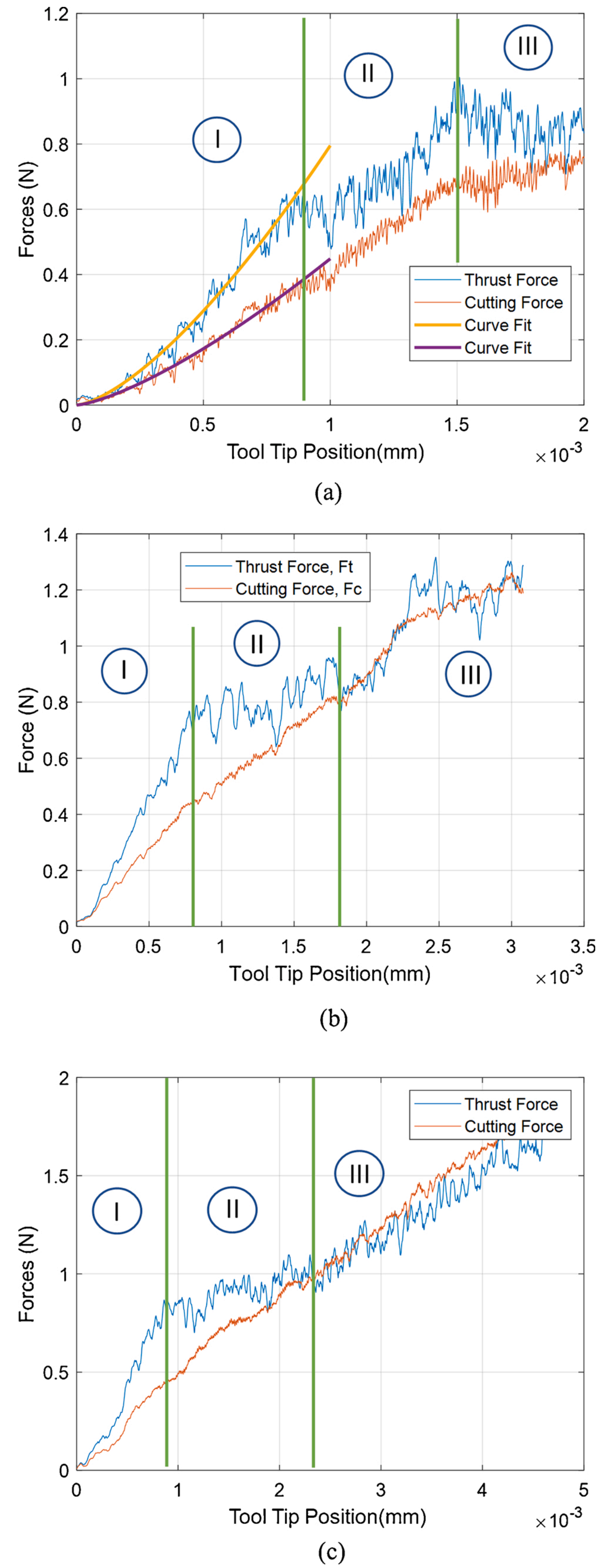

Fig. 11. Force measurements for: (a) 2 μm amplitude case where no complete chip formation was observed, (b) 3 μm amplitude case with chip formation, (c) 5 μm amplitude case with chip formation as indicated in Region III.

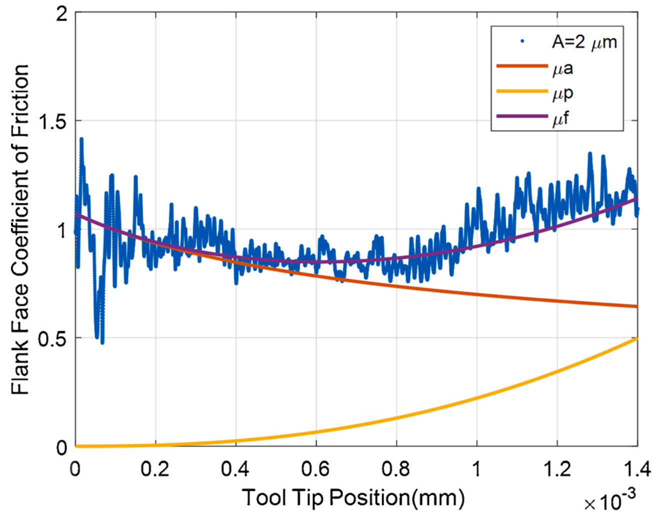

(a)

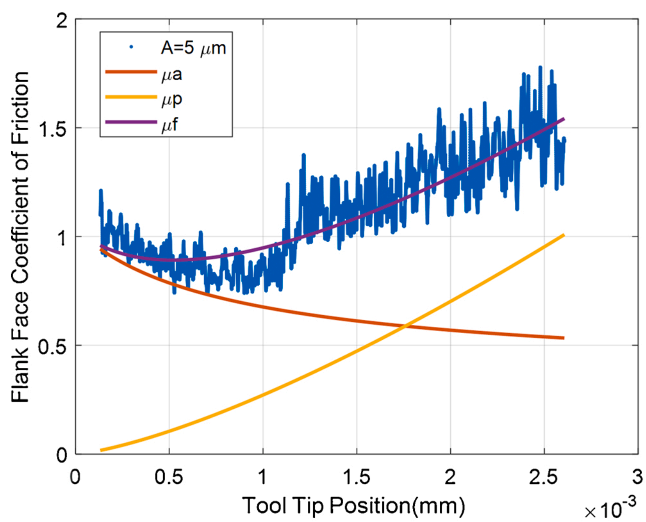

(b)

Fig. 12. Measured flank face coefficient of friction and identified adhesion and deformation components of the friction (a) A = 2 μm, (b) A = 5 μm.

Table 2

Identified coefficients with $H_0 = 2$ GPa, $\tau 0 = H_0/(3\sqrt{3})$ GPa, $h_s = 0.55$ μm, $h_w = 0.8$ μm, $l_s = 5$ μm.

Amplitude (μm)	C_a	C_p	m
2	1.75	10.89	1.484
3	1.78	9.9	1.85
5	1.79	10	1.37

for all experimental cases.

The rake face coefficient of friction formulation in Eq. (11) assumes that the ploughing forces remain constant after chip formation. However, the functions shown in Fig. 12 are increasing within Region II. A portion of that increase must be due to forces acting on the rake face of the tool due to material pile up just before the chip formation. If ploughing forces identified in Region I are subtracted from measured thrust and cutting forces, variation rake face coefficient of friction for 5 μm amplitude is shown in Fig. 13. Rake face coefficient of friction stabilizes around 0.7 after chip formation starts. High coefficient of friction during chip formation can be related to adhesion, and the role size effect must be considered similar to flank face contact conditions.

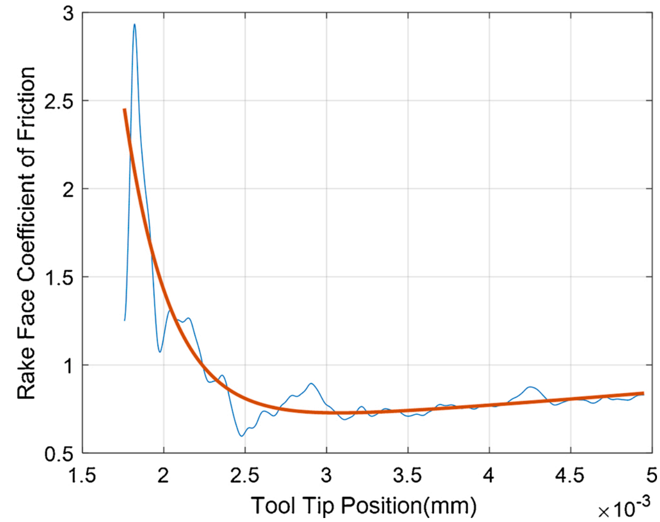

Fig. 13. Variation rake face coefficient of friction as function of tool tip position for 5 μm amplitude case.

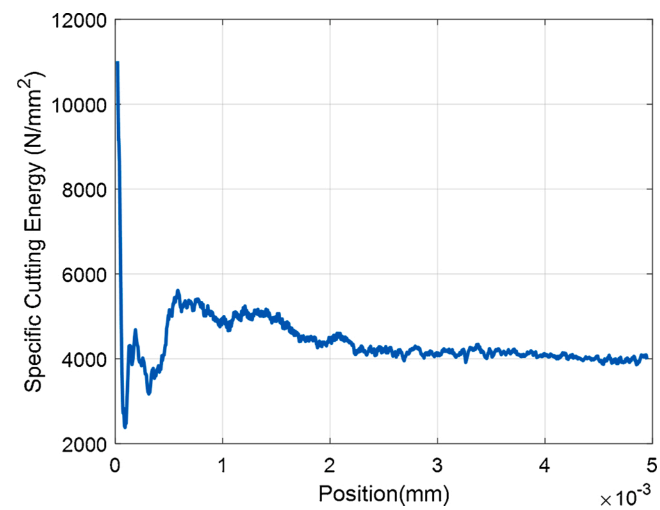

Fig. 14. Specific cutting energy for 5 μm amplitude cutting test.

The high friction at the first contact on the flank face and on the rake face during transition from material pile-up to chip formation region must influence the specific cutting energy. Fig. 14 shows the specific cutting energy calculation for 5 μm amplitude case, where two peaks can be observed due to small cutting edge radius of the diamond cutting tool. Such curves are common when pure metals are tested with nano indentation as well (Voyiadjis and Peters (2010)). The first peak can be related to the initial contact with flank face, and the second corresponds to Region II. The region in between, where specific cutting energy decreases, can be related to different length scales of the material and the contact conditions between the tool and the resulting surface topology. Similar observations were made by Rahman et al. (2020) this behavior was explained as switch between shearing to extrusion process which implies a significant contact on the flank face and Feng and Sagapuram (2021) emphasized the importance of adhesion at the tool-chip interface

When edge radiused tools are used in micro machining, minimum uncut chip thickness is usually found in the range of 25–50 % of the edge radius as shown in Budak et al. (2016). The edge radius affects the material flow around the cutting edge and influences the surface topology of the machined surface. Hence, a different balance between adhesion and deformation would take place on the flank face. The friction testing and analysis methodology presented in this study is promising and can be extended to study the influence of cutting edge radius on the machining process. This approach together with the ability to investigation specific grain deformations as in Ahmadi et al. (2018) would give plenty of information about the deformation mechanics of hcp materials. A better understanding of the flank face contact is crucial for shedding light onto surface generation mechanisms, which is an issue that is paramount in precision machining.

7. Conclusions

In this study, an experimental method was developed to investigate the flank and rake face friction during precision machining of commercial pure titanium alloy. An orthogonal plunge-in/pull-out test scheme, performed on an ultra-precision CNC that allows for studying flank and rake face coefficient is considered. A micro scale diamond tool was used to simplify the problem by eliminating the influence of edge radius and decrease the influence of temperature rise on the results. The test setup allows to reach practical cutting speeds. In addition, mechanical properties of the work material were investigated with nano indentation tests, whose results were integrated into the friction model to study the contribution of adhesion and deformation on the flank forces. The findings of the study for the single crystal diamond vs cp-Ti tribo-pair can be summarized as:

- The friction model proposed in this study can capture the variation in the flank face coefficient of friction considering the size effects. The size effect information obtained from nano indentation and cutting experiments was used to separate adhesion and deformation components of the flank face friction.
- The influence of adhesion is observed to be higher than deformation for the diamond tools used in this study. As tool plunges-in further, the influence of deformation increases. Flank face surface topology seems to affect adhesion and improve the surface quality.
- The best surface quality corresponds to Region I-II, where frictional conditions together with the applied pressure distribution leads to a favorable surface roughness for 3 μm amplitude case.
- The nanometer level cutting edge radius of SCD diamond tool alone did not eliminate the ploughing forces due to large contact conditions. The cutting force measurement did not present a positive intercept on the force curve.
- The influence of flank and rake face friction on size effect is shown by the results.

In future studies, the methodology presented here can also be used to investigate different work–tool material tribo-pairs as well as the influence of cutting tool edge radius and tool coating to analyze flank face friction mechanism during micro cutting. Another aspect of this approach of interest to future research would be to investigate simultaneously the friction and the materials' mechanical response. Cut chip thickness measurements can be used to calculate the shear strength of the material at high strain and strain rates, which can then be used to improve material constitutive models that are crucial to gaining predictive ability on machining processes.

CRediT authorship contribution statement

Yiğit Karpat: Conceptualization, Methodology, Data curation, Writing – original draft, Visualization, Investigation, Writing – review & editing, Funding acquisition.

Declaration of Competing Interest

The authors declare the following financial interests/personal relationships which may be considered as potential competing interests:

Yigit Karpat reports financial support was provided by Scientific and Technological Research Council of Turkey.

Acknowledgments

The author would like to thank Turkish Scientific Foundation Tubitak through project 218M431. The author would also like to thank Mr. Can Güven for his help during experiments.

References

Ahmadi, M., Karpat, Y., Acar, O., Kalay, Y.E., 2018. Microstructure effects on process outputs in micro scale milling of heat treated Ti6Al4V titanium alloys. J. Mater. Process. Tech. 252, 333–347.
Albrecht, P., 1960. New developments in the theory of the metal-cutting process: part I. The ploughing process in metal cutting. J. Inst. Eng. 82 (4), 557.
Arcona, C., Dow, T.A., 1998. An empirical tool force model for precision machining. J. Manuf. Sci. Eng. 120 (4), 700–707.
Bhushan, B., Nosonovsky, M., 2004. Comprehensive model for scale effects in friction due to adhesion and two- and three-body deformation (plowing). Acta Mater. 52, 2461–2474.
Budak, E., Ozlu, E., Bakioglu, H., Barzegar, Z., 2016. Thermo-mechanical modeling of the third deformation zone in machining for prediction of cutting forces. CIRP Ann. Manuf. Technol. 65, 121–124.
Childs, T.H.C., 2010. Surface energy, cutting edge radius and material flow stress size effects in continuous chip formation of metals. CIRP J. Manuf. Sci. Tech. 3, 27–39.
Feng, G., Sagapuram, D., 2021. A strong basis for friction as the origin of size effect in cutting of metals. Int. J. Mach. Tools Manuf. 168 (Part B), 103741.
Greenwood, J.A., Williamson, J.B.P., 1966. Contact of nominally flat surfaces. Proc. R. Inst. 295, 1442.
Huang, Y., Zhang, Hwang, K.C., Nix, W.D., Pharr, G.M., Feng, G., 2006. A model of size effects in nano-indentation. J. Mech. Phys. Solids 54, 1668–1686.
Kieren-Ehses, S., Böhme, L., Rivas, L.M., Lösch, J., Kirsch, B., Kerscher, E., Kopnarskic, M., Aurich, J.C., 2021. The influence of the crystallographic orientation when micro machining commercially pure titanium: a size effect. Precis. Eng. 72, 158–171.
Liu, K., Melkote, S.N., 2007. Finite element analysis of the influence of tool edge radius on size effect in orthogonal micro-cutting process. Int. J. Mech. Sci. 49, 650–660.
Lucca, D.A., Seo, Y.W., Komanduri, R., 1993. Effect of tool edge geometry on energy dissipation in ultraprecision machining. CIRP Ann. 42 (1), 83–86.
Lütjering, G., Williams, J.C., 2007. Titanium, 2nd edition. Springer.
Melkote, S.N., Grzesik, W., Outeiro, J., Rech, J., Schulze, V., Attia, H., Arrazola, P.J., M'Saoubi, R., Saldana, C., 2017. Advances in material and friction data for modelling of metal machining. CIRP Ann. - Manuf. Tech. 66, 731–754.
Novikov, N.V., Dub, S.N., Milman, Y.V., Gridneva, I.V., Chugunova, S.I., 1996. Application of nanoindentation method to study a semiconductor-metal phase transformation in silicon. J. Superhard Mater. 18, 32.
Persson, B.N.J., Scaraggi, M., 2014. Theory of adhesion: role of surface roughness. J. Chem. Phys. 141, 124701.
Rahman, M.A., Woon, K.S., Venkatesh, V.C., Rahman, M., 2018. Modelling of the combined microstructural and cutting edge effects in ultraprecision machining. CIRP Ann. 67 (1), 129–132.
Rahman, M.A., Rahman, M., Mia, M., Gupta, M.K., Sen, B., Ahmed, A., 2020. Investigation of the specific cutting energy and its effect in shearing dominant precision micro cutting. J. Mater. Process. Tech. 283, 116688.
Ramos, A.C., Autenrieth, H., Strauß, T., Deuchert, M., Schulze, V., 2012. Characterization of the transition from ploughing to cutting in micro machining and evaluation of the minimum thickness of cut. J. Mater. Process. Tech. 212 (3), 594–600.
Shugurov, A., Panin, A., Dmitriev, A., Nikonov, A., 2018. The effect of crystallographic grain orientation of polycrystalline Ti on ploughing under scratch testing. Wear 408–409, 214–221.
Suh, N.P., Sin, H.C., 1981. The genesis of friction. Wear 69, 91–114.
Voyiadjis, G.Z., Peters, R., 2010. Size effects in nanoindentation: an experimental and analytical study. Acta Mech. 211, 131–153.
Zhao, Z., To, S., Zhu, Z., Yin, T., 2020. A theoretical and experimental investigation of cutting forces and spring back behaviour of Ti6Al4V alloy in ultraprecision machining of microgrooves. Int. J. Mech. Sci. 169, 105315.